

A large field CCD system for quantitative imaging of microarrays

G. Hamilton¹, N. Brown¹, V. Oseroff¹, B. Huey^{1,5}, R. Segraves^{1,5}, D. Sudar², J. Kumler³, D. Albertson^{1,4,5} and D. Pinkel^{1,5,*}

¹Comprehensive Cancer Center, University of California San Francisco, CA, USA, ²Lawrence Berkeley National Laboratory, Berkeley, CA, USA, ³Coastal Optical Systems, West Palm Beach, FL, USA, ⁴Cancer Research Institute, University of California San Francisco, CA, USA and ⁵Department of Laboratory Medicine, University of California San Francisco, CA, USA

Received February 13, 2006; Revised March 10, 2006; Accepted March 20, 2006

ABSTRACT

We describe a charge-coupled device (CCD) imaging system for microarrays capable of acquiring quantitative, high dynamic range images of very large fields. Illumination is supplied by an arc lamp, and filters are used to define excitation and emission bands. The system is linear down to fluorochrome densities $\ll 1$ molecule/ μm^2 . The ratios of the illumination intensity distributions for all excitation wavelengths have a maximum deviation $\sim \pm 4\%$ over the object field, so that images can be analyzed without computational corrections for the illumination pattern unless higher accuracy is desired. Custom designed detection optics produce achromatic images of the spectral region from ~ 450 to ~ 750 nm. Acquisition of a series of images of multiple fluorochromes from multiple arrays occurs under computer control. The version of the system described in detail provides images of 20 mm square areas using a 27 mm square, 2K \times 2K pixel, cooled CCD chip with a well depth of $\sim 10^5$ electrons, and provides ratio measurements accurate to a few percent over a dynamic range in intensity >1000 . Resolution referred to the sample is 10 μm , sufficient for obtaining quantitative multi-color images from $>30\,000$ array elements in an 18 mm \times 18 mm square.

INTRODUCTION

Quantitative fluorescence imaging is one of the critical steps in the long analytical chain that links the specimen to data in microarray experiments. While most microarray imaging systems employ scanned laser excitation coupled with

photomultiplier tube light detectors, an alternative approach employing wide field imaging and charge-coupled device (CCD) detectors has some very attractive features. Among the advantages of CCD systems are their high quantum efficiency, $>90\%$ across the visible and near infrared compared with 10–30% for photomultipliers, photometric linearity, and the ability to use broadband light sources coupled with filters to allow tailoring of the wavelength bands for any desired fluorochrome. However, wide field systems may have background light levels because light originating at any depth can reach the CCD, adequately uniform illumination of large areas is difficult and imaging large areas requires coordinated analysis of multiple images. In contrast, laser-scanning systems produce a continuous image of scanned areas of arbitrary dimensions, and discriminate against light originating out of the focal plane. But the depth of field limitation makes them sensitive to the flatness of the array surface unless dynamic autofocus-ing is employed (<http://www.chem.agilent.com/>).

A number of CCD-based imaging systems for microarray analysis have been built (1), and several are commercially available (AppliedPrecision <http://www.api.com/index.html>, Alpha Innotech <http://www.alphainnotech.com/>, Abbott Molecular Diagnostics <http://www.vysis.com/home.html>). These systems address the challenges of using CCD detectors in various ways, and make various compromises that affect their abilities to measure high-density arrays with high analysis rates over a large dynamic range. As part of a comprehensive microarray research program, we have built a series of CCD-based microarray imaging systems with superior performance compared to these instruments. We desired sensitive, photometrically accurate, high-dynamic range images to allow improved understanding of fundamental aspects of array hybridization and measurement, and operational convenience for large-scale biological applications. The design choices we have made are optimized for multi-fluorochrome comparative hybridizations from arrays on transparent or reflective substrates, where ratios of signals provide the basic

*To whom correspondence should be addressed. Tel: +1 415 476 3659; Fax: +1 415 476 8218; Email: pinkel@cc.ucsf.edu

information. We focus on ratio measurements since this is an effective method of compensating for production variation among arrays. The system we describe and characterize here acquired 16 bit images of 20 mm \times 20 mm areas with 10 μ m resolution, sufficient for obtaining accurate data from tens of thousands of array elements per field. Acquisition time for a multicolor image series under typical conditions is \sim 1 min per field. If more than one image is required for an array, we analyze them independently and merge the datasets. Here we describe the design goals and details of our imager, comprehensively evaluate its performance and discuss some general issues of array imaging that motivated our approach.

MEASUREMENT AND ANALYSIS PROCEDURES

The typical arrays imaged with this system consist of DNA solutions printed on either transparent glass or chromium-coated microscope slides. The chromium surface has the advantage of being reflective (reflectivity \sim 60%), which increases the signal intensities by a factor of \sim 2.5 and provides very low backgrounds. Moreover, it effectively limits the depth of field so that the glass substrate and fluorescent contaminants on the back surface of the slide do not produce background light in the image. However, the bare chromium surface profoundly quenches the emission from the fluorochromes if they are measured dry. The quenching can be avoided by mounting the arrays in a solution of 90% glycerol, 10% phosphate-buffered saline (PBS), pH \sim 8, and applying a standard glass coverslip. This mounting medium also contains the DNA stain DAPI. For arrays made from cloned DNA or PCR products, the density of printed DNA is sufficient so that the DAPI image can be used to automatically identify the array elements independent of the hybridization signals. Arrays made from oligonucleotides typically do not produce sufficient DAPI signal for segmentation so these elements are located based on the hybridization signals. No fluorescence antifade compounds are used for the arrays since these may produce substantial fluorescence. As shown below, bleaching is not an issue with this instrument. The same mounting medium is used for arrays on transparent substrates since we believe it improves the performance of the fluorochromes. A typical array measurement includes acquisition of a DAPI image in addition to images of each of the fluorochromes used label the nucleic acids in the hybridization.

Array images were analyzed using the software package UCSF SPOT (2). SPOT segments array elements based on either the DAPI image or the hybridization images, determines the intensities of the hybridization signals, corrects the intensities for local background, and calculates various measures of signal ratio and data quality based on the signal distributions within the elements. The measure of ratio for an array element used for all of the data in this paper is simply the quotient of the background-corrected total integrated intensities. No computational adjustments of any type have been applied to the images or the data, except for application of an overall normalization factor for display of genome ratio profiles. The effect of computational image sharpening is also illustrated in one figure.

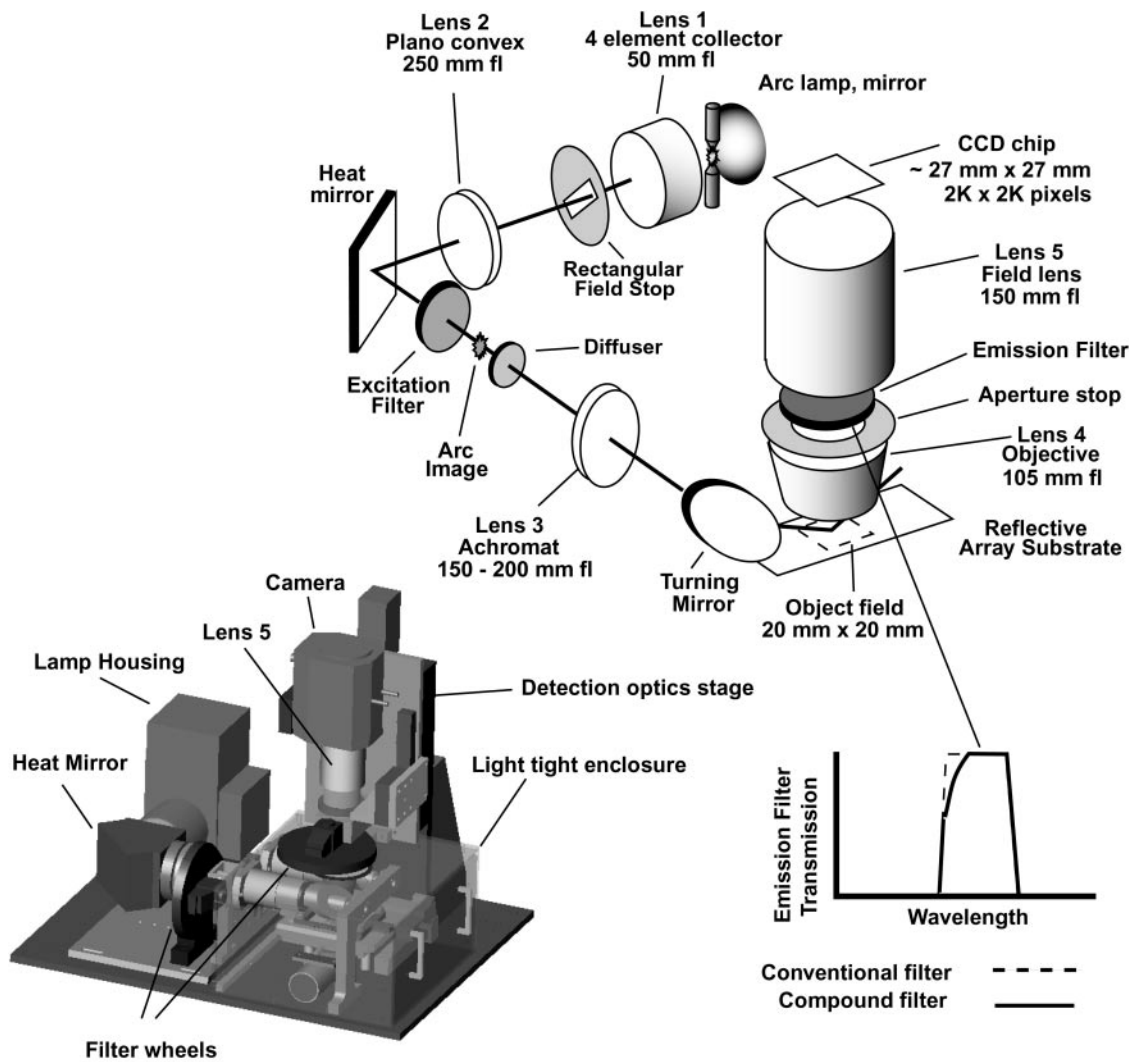
OPTICAL DESIGN

Excitation optical path

The primary design goals of excitation optics are production of a constant ratio of excitation intensities over the array for all fluorochrome combinations, and minimization of the amount of excitation light entering the detection optics in order to avoid production of fluorescence from the objective lens. These are accomplished using dark field Koehler illumination.

The essential components of the optical system are schematically shown in Figure 1, along with a CAD picture showing the actual configuration. Excitation light is supplied by a 200 W mercury-xenon lamp (Oriel 66011 housing) with a 4-element fused silica collector lens, 50 mm fl, 75 mm output diameter (Lens 1, Oriel Aspherab 66061), to produce a high-quality collimated light beam. A rectangular field stop, placed just after the output surface of the collector, is imaged onto the array by a lens pair consisting of a 250 mm fl, 75 mm diameter plano-convex BK-7 uncoated lens (lens 2) and a (typically) 150–200 mm fl, anti-reflection coated, achromatic doublet (lens 3). These two lenses are separated by the sum of their focal lengths. An image of the arc is produced in the mutual focal plane between these two lenses. A 0.5° holographic diffuser (Physical Optics Corporation, Torrance CA) is located just after the arc image. The diffuser blurs high spatial frequency variations in the illumination pattern due to imperfections in the envelope of the arc lamp and reflections among the optical elements. An infrared-transmitting turning mirror (transmission for $\lambda > 1000$ nm at 45° incidence; Chroma Technology, Rockingham VT; Oriel 66247 mount and heat sink) is used to remove heat from the beam to protect the excitation filters, and to fold the light path to reduce the footprint of the instrument. Excitation filters, 32 mm diameter (Chroma Technology, Rockingham VT) mounted in a 10-position filter wheel (TOFRA 007-00; Palo Alto CA) are located prior to the arc image so that the remaining heat load in the beam is spread over a large area of the filter. The angle of convergence of the excitation light at the filter is small enough, $<6^\circ$, so that the spectral properties of the filter are constant for the entire beam. An electronic shutter (Unibiltz Rochester NY) prior to the filter blocks the excitation beam except during image acquisition.

A turning mirror directs the collimated excitation beam down onto the horizontally mounted array at angle \sim 45° from the normal. The aspect ratio of the rectangular field stop, \sim 1.4, and its orientation about the optical axis are chosen to produce a square illumination pattern on the array. The dark field illumination path and the use of light absorbing materials and baffles to capture scatter from imperfections in the optical elements substantially eliminate the entrance of excitation light into the detection objective (Lens 4), thereby avoiding background light in the image due to fluorescence from the lens elements. Excitation light that is diffusely scattered by the array surface cannot be blocked from entering the detection optics, but its intensity is low enough so that it does not excite significant emission from the objective. However, the diffusely scattered light may cause other problems, which are dealt with as discussed below. Measurements of background light levels in the instrument are discussed below and illustrated in Figure 2.



Filter Characteristics			
	Ex	Em	Ex Intensity (mW/mm ²)
DAPI	360/40	450/40	
Fluorescein	495/15	530/30	0.02
Cy3	546/11	567/15	0.11
Texas red	577/15	608/23	
Cy5	635/30	680/40	0.04

Figure 1. Overview of the optical design. The major optical components of the instrument are shown in the sketch and their function is described in the text. The actual configuration of the system is shown in the CAD picture, including the light tight enclosure and the motorized stage for array transport. The drawing of the band pass of a representative emission filter shows the shape of the transmission curve of a normal interference filter, and for the compound filters used in this instrument which also contain a layer of absorbing glass to block transmission of scattered light that may be incident on the filter at large angles from the normal. The characteristics of the excitation and emission filters are listed in the table, as are representative intensities of the excitation light.

After illuminating the array, the excitation beam is usually absorbed in a stop, but can be reflected back onto the array, thereby increasing the excitation intensity by ~50%. The reflection system consists of a 150 mm fl achromatic doublet with a mirror 150 mm behind it. The lens is placed ~150 mm from the centerline of the array. The locations of the reflector or beam stop depend on whether reflective or transparent array substrates are used.

The dimensions of the rectangular field stop are adjusted to provide useful illumination of an area of 20 mm × 20 mm. This

requires illuminating a somewhat larger area so that the intensity roll off due to the blurring caused by the diffuser does not begin until beyond the object field. When lens 3 has a focal length of 200 mm, the dimensions of field stop are 23 mm × 30 mm (diagonal dimension ~37 mm). Thus only about half of the diameter of the ~75 mm output beam from the collector lens is being used. Decreasing the focal length of lens 3 and correspondingly increasing the size of the field stop to maintain the same illumination area increases the excitation intensity proportionally to $\sim 1/f^2$. However, increased aberrations in

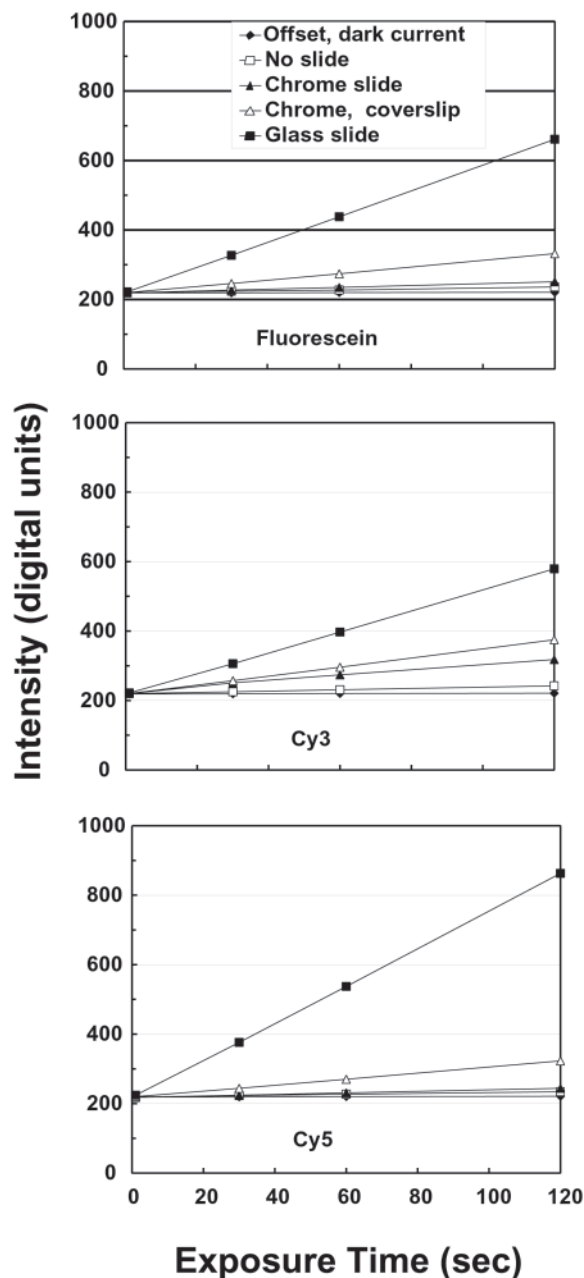


Figure 2. System offset and background light levels as a function of exposure time for various measurement conditions. Intensity at the center of the image as a function of exposure time is shown for the system when no array is present, and for a bare chromium substrate, a chromium substrate plus coverslip and a glass slide. In addition the camera output with the excitation light off is also shown to demonstrate the camera offset and dark current. The key to identify the various curves is located in the upper graph, which shows backgrounds for the fluorescein filter set. The middle and lower graphs provide similar information for the Cy3 and Cy5 filter sets, respectively. The data show that the camera offset is ~ 220 U, and that the dark current of the camera is negligible over these integration times. These curves allow estimation of the background light levels due to the array substrate and mounting components. For example, typical integration times for our measurements are 20–40 s for Cy3 and Cy5, which result would result background contributions of 20–50 digital units for the chrome slide plus coverslip in an actual array measurement. Background for the standard glass slides are much higher, and are variable among batches of slides perhaps due to trace differences in their compositions. Total backgrounds in real array measurements will be higher than in this figure due to non-specific binding during the hybridization. Figure 9 shows the effect backgrounds on measurement precision.

the collector lens farther from the center of the excitation beam result in increased illumination non-uniformity and chromatic dependence of the illumination pattern. Moreover, we have noted a wavelength-dependent change in the angular emission pattern of the lamp as it ages, presumably due to asymmetric build up of UV damage in the lamp envelope because of position-dependent intensity variation within the arc. This increases variation in the illumination pattern as the excitation wavelength is changed. Limiting the angular range of emitted light used for illumination of the specimen maintains the desired uniformity specifications for a longer operating time for each lamp. Measurement of the illumination uniformity is discussed below and illustrated in Figure 3. Typical useful lamp life is 500–1000 h.

Detection optical path

The primary design goal of the detection optics is to provide an achromatic, well-focused image of the entire object field with a resolution of $\sim 10 \mu\text{m}$ over a useful wavelength range of ~ 450 to ~ 750 nm.

The telecentric detection optics shown in Figure 1 were designed and fabricated by Coastal Optical Systems (West Palm Beach, FL). Each lens contains multiple elements fabricated from three or four different materials. All surfaces have high performance anti-reflection coatings, and the internal structural components of lenses have been treated to reduce light scatter. The objective lens (lens 4) collects and collimates light emitted from the array, and the field lens (lens 5) focuses the parallel light to form an image on the CCD chip. The magnification of the system is the ratio of the focal lengths of the two lenses. This design provides very uniform detection sensitivity over the entire field, the calculations indicating variation $< 2\%$.

The set of lenses designed and built for this system include objectives with focal lengths of 75 mm (Coastal Optical 99044-75), 105 mm (Coastal Optical 02244) and 150 mm (Coastal Optical 99044-150), and a field lens with a focal length of 150 mm (identical to the 150 mm objective). These lens combinations provide magnifications of $2\times$, $1.4\times$ and $1\times$ with maximum light collection capabilities of $f/2.3$, $f/3.3$ and $f/4.7$, respectively. The object fields of the objectives are suitable for acquiring images of 12, 18 and 25 mm square arrays. The image field has a diameter of 36 mm, for use of CCDs with large numbers of pixels and high-electron capacity. The entire detection system is mounted on a large precision manual translation stage for focusing, and for positioning the detector to accommodate the large size differences of the objectives.

The system whose performance is documented in detail in this paper uses the $1.4\times$ magnification lens set and acquires images of ~ 20 mm square fields on a $27 \text{ mm} \times 27 \text{ mm}$ square back-thinned, anti-reflection coated, thermoelectrically cooled (-75°C) CCD chip with $2\text{K} \times 2\text{K}$ pixels (Andor Technology DW436N-BV). This provides a $10 \mu\text{m} \times 10 \mu\text{m}$ pixel size referred to the object. Maximum quantum efficiency of the chip is 95% and its well depth is $\sim 100\,000$ electrons. Output is digitized to 16 bits. The camera readout rate is 1 MHz, resulting in a 4 s readout time for the full image. The calculated polychromatic resolution of the optics is better than the pixel size across most of the image, and matches it in the corners.

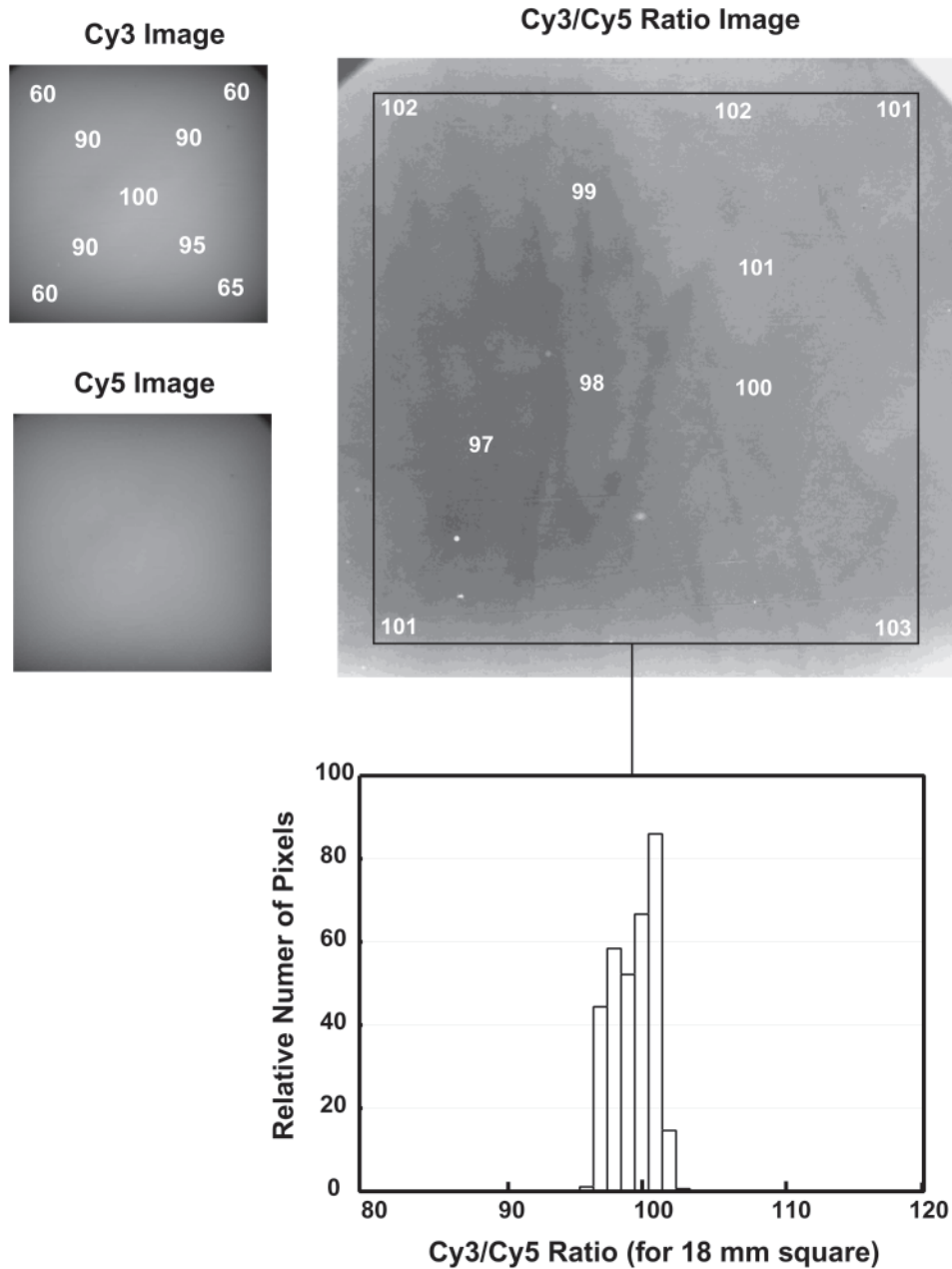


Figure 3. Illumination distributions over the object field. Images of fluorescence from a smoky gray translucent plastic test sheet were obtained using the Cy3 and Cy5 filter sets. The intensity pattern in the image directly indicates the illumination pattern because the detection optics provide essentially uniformity of the sensitivity over the field. At the left, images of the full-field illuminations for Cy3 and Cy5 are shown, with the relative intensities at representative locations in the field indicated. The intensities are highest in the center, and drop to ~60% of the central value at the corners of the 18 mm area used for array imaging. The dark areas at upper left and upper right corners of the images are due to obstruction of the light path by the boundaries of the open camera shutter. The (linear) ratio of these two images, smoothed using a median filter with a radius approximately the size of an array element (3 pixels) and contrast-stretched so that 1% changes result in a change in gray level, is shown to the right. Relative (linear) ratio values for the various gray levels are indicated on the image within a black boundary that indicates the area of an 18 mm square array. A histogram, bottom, of the intensity values within the 18 mm square shows that the full range of this distribution is $\pm 4\%$, with most of the image within $\pm 3\%$.

The lens system produces a relatively shallow depth of field at the image plane, making it necessary to provide multi-axis adjustability in the camera mount so that the CCD chip can be oriented accurately orthogonal to the optical axis in order to have the entire image in focus. The large diameter of the light bundle entering the camera necessitates use of a faceplate with a larger opening than is standard in order to avoid clipping light in the corners of the image.

Emission filters, 32 mm diameter, and an adjustable aperture are located at the mutual focal plane between the two lenses so that changing the aperture uniformly affects the light collection over the entire image. The filters are held in a 10-position filter wheel identical to the one used for the excitation filters. The band passes of the filters, listed in Figure 1, are primarily determined by interference structures that are designed for normal incidence. As the angle of incidence

exceeds $\sim 10^\circ$, the transmission band moves significantly to shorter wavelengths. The optics are designed so that all of the fluorescent light is incident on the filter at $< 7^\circ$ from the normal so that the band pass is constant for all parts of the image. However, some of the stray excitation light that enters the objective lens may be scattered from the internal lens structures even though they have been treated to reduce scatter, and thus be incident on the filter at sufficiently high angles from the normal that it will pass through an interference filter. To block this light we use custom designed filters (Chroma Technology, Rockingham VT) that contain a colored glass layer in addition to the interference structures. This slightly reduces the transmission of the filters, most prominently rounding the shape of the pass band on the low wavelength side, as illustrated in Figure 1. The filters have highly parallel surfaces so that images of all fluorochromes are registered to a fraction of a pixel.

The surfaces of the filters have anti-reflection coatings in order to reduce backgrounds. Fluorescence that may be reflected from the filter returns to the array substrate, where it forms an in focus mirror image of the array. A portion of this light may be reflected from the array substrate, re-entering the detection optics and producing a weak 'ghost' image on the CCD. Ghosts are especially noticeable when using reflective array substrates such as those with our standard chromium coating. The ghosts are a fraction of a percent of the intensity of the primary image, and only cause difficulty if the ghost of a very bright array element or contaminating particle occurs near the primary image of a weakly fluorescing array element. To reduce interference from the ghosts to an insignificant level we defocus them by positioning the CCD chip several millimeters closer than one focal length from the field lens, which results in the primary image of the array being in focus when it is slightly farther than one focal length from the objective. This small amount of 'non-ideal' positioning of the lenses does not significantly degrade the primary image. The defocused ghost then contributes a slowly varying background to the primary image, which can be accurately subtracted during image analysis.

Arrays are mounted on a motorized stage (TOFRA Inc. 006, Palo Alto, CA) using a custom-built precision holder that places the array elements at a reproducible distance from the detection optics. Once the system has been focused, all portions of all arrays in the holder can be imaged without adjustment. Similarly, refocusing is not required when the holder is reloaded with a new set of arrays. The current stage can accommodate three microscope slides, each containing multiple arrays.

Image acquisition

Images are acquired under control of a commercial software package (QED InVivo; Media Cybernetics, Silver Springs, MD, USA). The software, originally intended to operate fluorescence microscopes, has been modified slightly to accommodate the specific components and image acquisition sequence of the array imager. Arrays are positioned under the objective lens either by manual switch stick control or by commanding the stage to move to a preset position. A series of positions can be defined so that all images for the arrays in the holder can be acquired automatically. At each location an image of each

fluorochrome is acquired in sequence by moving the filter wheels to appropriate positions, opening the excitation shutter, integrating the emitted fluorescence for the preset time, closing the shutter, reading out the camera and repeating the cycle for each of the desired fluorochromes.

SYSTEM PERFORMANCE

Background light levels

The combination of dark field illumination, careful baffling to control scattered light and the compound emission filter design results in a system with very low backgrounds. Figure 2 shows the background intensity as a function of exposure time for a variety of measurement configurations. The camera output when no excitation light is present, consisting of camera baseline offset plus dark current, is also shown for comparison. Note that the dark current is insignificant. The background produced by a bare reflective chrome slide is only slightly higher than the baseline offset of the camera, but glass components such as coverslips and glass slides produce higher backgrounds due to their intrinsic fluorescence. Some coatings used on slides to bind nucleic acids increase the background level substantially. Backgrounds from coatings are equally present in laser-scanning imagers since they are not removed by depth discrimination. Uniform background levels of this type can be accurately subtracted, but statistical noise from them can reduce measurement precision at low intensities, as discussed below and illustrated in Figure 9.

Ratio uniformity

The illumination characteristics of the system for Cy3 and Cy5 are shown in Figure 3. While the illumination intensities in the corners drop to $\sim 60\%$ of value near the center of the field, the ratio is constant to $\pm 4\%$ across the full area of an 18 mm square array. Given this performance, we do not routinely correct for spatial variation in data introduced by the illumination distribution when analyzing multicolor ratio hybridizations. If one wanted to compare single-fluorochrome intensity measurements for arrays measured at widely different times, then a flat field correction for the illumination pattern would be required because the details of the pattern drift, in part due to changes in the arc and lamp envelope as lamps age.

Image quality

Figure 4 shows full-frame image of an England Finder test slide, and expanded views of the center and corner of the image. This indicates that the object field is ~ 20 mm \times 20 mm. There is a slight radial softness in the image in the corners of the field, but it is imperceptible in this figure. Images of a test slide containing 1 μ m diameter fluorescent beads (Molecular Probes/Invitrogen, Carlsbad, CA) show that if a bead is centered in a pixel, the nearest neighbor pixels have $\sim 20\%$ of the intensity of the center (data not shown). Thus, approximately half of the total intensity emitted from this sub-resolution object falls within the central pixel so that the optical resolution is well matched to the pixelization of the image.

Figure 5 shows the DAPI image, ~ 1 s exposure, of an 18 mm \times 18 mm test array containing ~ 32 000 elements

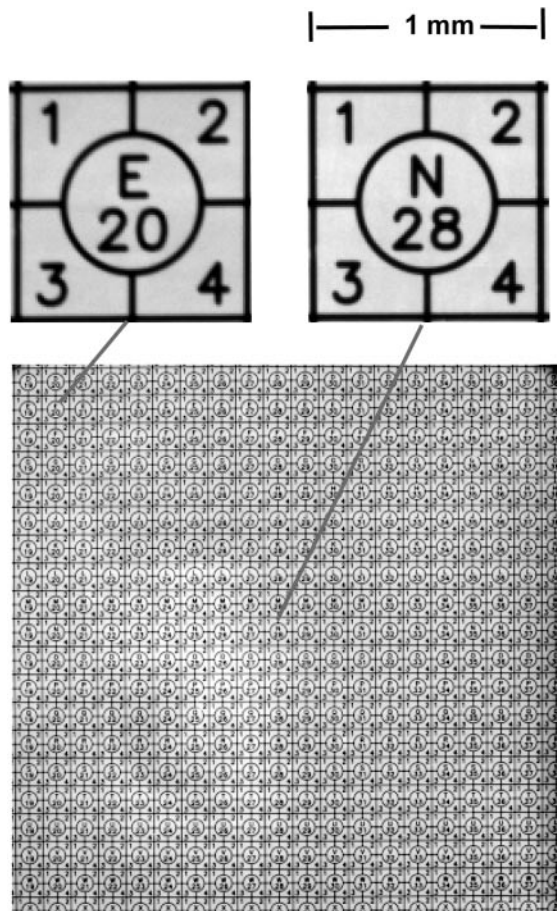


Figure 4. Resolution across entire image. Full-frame image of an England Finder slide consisting of etched 1 mm squares on a thick glass substrate. The image was obtained using the Cy5 filter set. The excitation light produced fluorescence in the glass substrate, which back-illuminate the etched pattern on the upper surface. Enlarged images of two of these squares, one at the center and one at a corner, are shown, indicating that the focus is maintained across the entire field. The full-field encompasses approximately a 20 mm square, which given the $2K \times 2K$ pixels, calibrates the pixelization as $10 \mu\text{m}/\text{pixel}$.

printed on $\sim 95 \mu\text{m}$ center-to-center spacing using our custom-built printer (S. Clark, G. Hamilton, N. Brown, V. Oseroff, R. Nordmeyer, D. Albertson, D. Pinkel, manuscript in preparation). The insets show details of the image at the center and a corner, and plots of the intensities along a line of pixels through the spots in a corner of the field. Intensity traces are shown for both the original image and after computational sharpening using the measured point spread function of the optics. The original image is sufficiently sharp throughout for quantitative analysis, indicating that $\sim 20 \mu\text{m}$ between the points of closest approach for neighboring array elements is sufficient for accurate measurements. However, computational sharpening may allow measurements at even closer spacing between elements.

Sensitivity

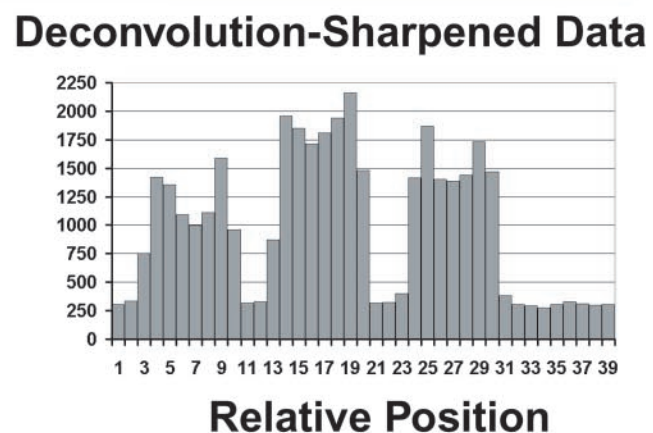
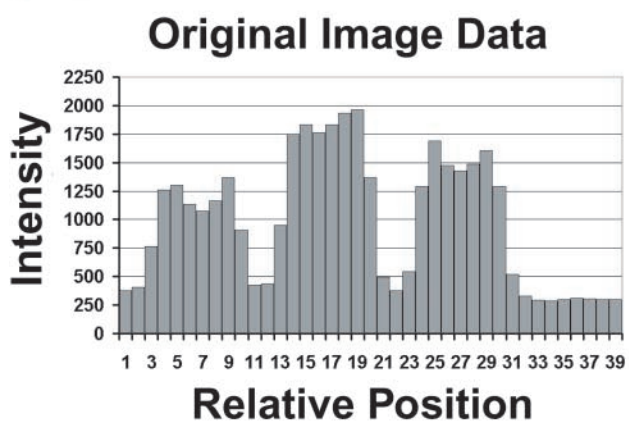
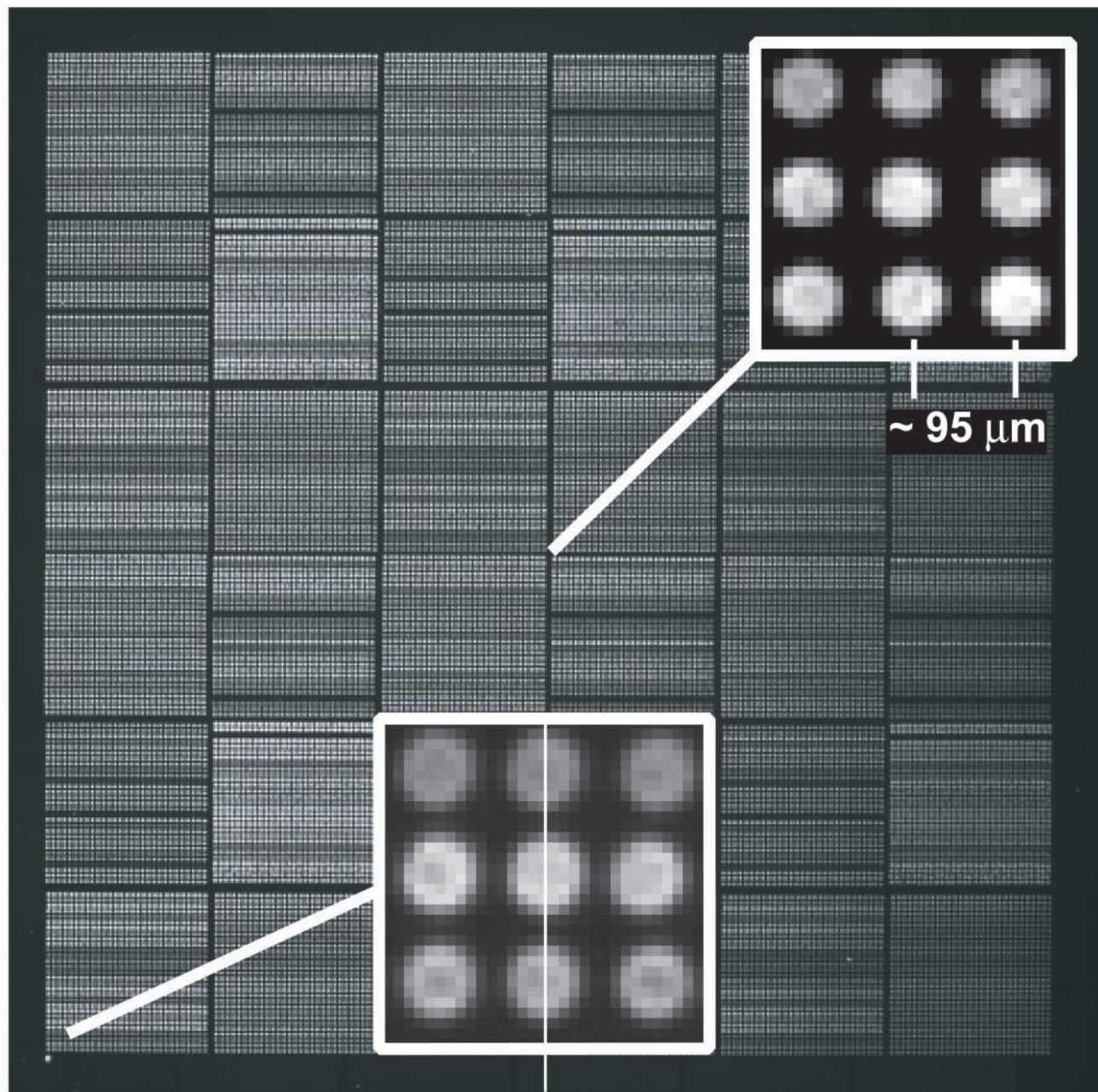
The sensitivity of the imaging system was evaluated by closely simulating the measurement environment of our

arrays. Solutions containing various concentrations of Cy3 and Cy5 in the glycerol/10% PBS medium we use for slide mounting were loaded into rectangular fused silica capillaries of interior dimensions $20 \mu\text{m} \times 200 \mu\text{m}$ (Vitrotubes #5002S-050; VitroCom, Mountain Lakes NJ), and the capillaries were mounted on a chromium array substrate, as shown in Figure 6a. Fused silica was used because of its low fluorescence, and fluorochromes directly conjugated to dCTP nucleotides were used as a partial simulation of the attachment to DNA. Measured fluorescence intensities depend linearly on the fluorochrome density, and indicate the ability to obtain quantitative data at densities well below $1 \text{ fluorochrome}/\mu\text{m}^2$, Figure 6b. The sensitivity limit was set by non-uniform background 'clutter' due to emission from other sources in the measurement environment, not by the ability to detect the desired fluorescence.

Photo bleaching

The bleaching rate of signals from a hybridized array was determined by acquiring images of an array using standard exposure times (20 s Cy3, 40 s Cy5) periodically during an extended total period of exposure of 640 s for Cy3 and 1280 s for Cy5. Median signal intensity for elements on the array decreased linearly with time, with a total decrease of $\sim 1\%$ in Cy3 and 9% in Cy5. Assuming that these measurements represent the beginnings of an exponential decay, the estimated half-lives of the fluorochromes are $>10 \text{ h}$ exposure for Cy3, and $\sim 1.25 \text{ h}$ exposure for Cy5. Thus arrays can be measured multiple times if desired without concern for bleaching. The data in Figure 7 demonstrate that minimal bleaching occurred during the multiple measurements, which totaled several minutes of exposure.

There are several factors that probably contribute to the much reduced bleaching during image acquisition in this CCD system compared with typical laser-scanning microarray imagers. These include the somewhat lower total excitation doses and dramatically lower instantaneous excitation intensities in the CCD system. While accurate comparisons are difficult to make without full details of proprietary optical designs, laser systems typically employ 20 mW lasers for excitation and scan 1200 mm^2 areas in $\sim 8 \text{ min}$. Thus the energy 'dose' of the fluorochromes is $\sim 8 \text{ mJ}/\text{mm}^2$ for Cy3 and Cy5. If the laser beam is focused to a $10 \mu\text{m}$ spot, then the intensity during excitation is $2 \times 10^5 \text{ mW}/\text{mm}^2$. In contrast, this CCD system employs excitation intensities of ~ 0.11 and $0.04 \text{ mW}/\text{mm}^2$ for Cy3 and Cy5, respectively (table in Figure 1) and corresponding typical exposure times of 20 and 40 s. Thus the doses during a typical scan are 2.2 and $1.6 \text{ mJ}/\text{mm}^2$, several times lower than in a laser scanner. Even with the low excitation intensities, data acquisition rates can be very rapid. With an array of 30 000 elements as in Figure 5, the lowest acquisition rate, which occurs for the 40 s Cy5 exposure, corresponds to 750 array elements/s. As shown in Figure 8, arrays can have sufficient intensity so that 10-fold lower exposure times are practical, leading to correspondingly higher acquisition rates. The use of the glycerol/PBS measurement environment may also contribute to the reduction in bleaching in our measurements.



Fluorescence cross talk

The cross talk among fluorochromes is function of both the excitation and emission filter band passes. We have used filters intended to provide high levels of discrimination at the sacrifice of intensity. The cross talk of the system was measured by preparing capillaries as shown in Figure 6a, each filled with a 1 mM concentration of fluorescein-dCTP, Cy3-dCTP or Cy5dCTP. These were mounted on the same slide and images containing the three capillaries were obtained with the filter sets for each of the fluorochromes. Exposures were adjusted so that the image of each fluorochrome with its 'proper' filter set was close to camera saturation. The intensities of the other capillaries were then measured and normalized to that value. In most cases the signal from one fluorochrome produced using the filter set for another fluorochrome was below measurement threshold, indicating the cross talk was $\ll 10^{-4}$. The only two combinations with measurable cross talk were fluorescein, which produced a relative signal of 7×10^{-4} when viewed with the Cy3 filters, and Cy3, which produced a signal of 4×10^{-3} when using the fluorescein filters. Slight adjustments of filter the band passes could reduce these values. Examination of the excitation and emission spectra of Texas red (and its spectral equivalents) shows that with the filters listed in Figure 1 this fluorochrome will have significant cross talk with Cy3 and Cy5, but will be highly discriminated from fluorescein.

Microarray measurements

Figure 7a shows the results of an array CGH analysis of Cy3-labeled 'test' genomic DNA from a normal human female, and Cy5-labeled 'reference' genomic DNA from a normal male. The hybridization was performed as described by Snijders *et al.* (3) using a microarray of BAC clones (Humarray 3.1) obtained from the UCSF Cancer Center Microarray Core facility (<http://cc.ucsf.edu/microarray/>). The images were analyzed using the program SPOT (2), as described above, and the data from the triplicate elements representing each genomic locus were averaged. The Log_2 Ratios at the ~ 2500 loci are essentially constant, with a SD of 0.06, except for the expected alterations for the X and Y chromosomes at the right edge of the plot. An overall normalization factor was applied to set the median Log_2 ratio equal to zero.

Figure 7b shows the relationship of the Log_2 Ratio and signal intensity for all ~ 7500 array elements for the data set of Figure 7a. The ratio, M , is independent of intensity, A , as indicated by the highly elongated horizontal cluster of points corresponding to autosomal loci. Loci on the X chromosome fall above the autosomal distribution, while those on the Y are below it. Two additional datasets, obtained from this same

hybridization but 3-fold increases of either the Cy3 or Cy5 exposure times, are also shown. These data points move to new locations on the plot by exactly the amount that is expected based on the exposure alterations. Moreover, close examination of small features of the distributions show the high accuracy with which relative ratios are reproduced, even as large overall changes in the ratio are occurring due to the altered exposure times. These results demonstrate that the spatial uniformity and the linearity that were found in the various test procedures discussed above are achieved in real measurements. In routine measurements we make no attempt to balance the signal intensities in the different fluorochrome channels, because the linearity of the measurement system assures inter-comparability of datasets from different arrays measured at different times and with different intrinsic intensities.

Noise and dynamic range in array measurements

Two types of 'noise' can be introduced by an imaging system. The first is a time-independent, spatial variation in response that produces systematic differences in intensities and ratios depending on the location of an array element in the image. In a CGH measurement this spatial variation translates into variation in ratio as one moves along the genome, with the pattern depending on the mapping that relates the position of an element on the array to its genomic location. As shown in Figure 3, this imaging system can operate so that the maximum ratio variation over the imaged area is $< \pm 4\%$ on a linear scale, which is small but detectable in good datasets. This variation can be corrected computationally if higher accuracy is desired.

The second class of noise is stochastic, causing variation among repeated 'identical' measurements. In a CCD system the basic sources of such noise are fluctuations in the illumination, camera dark current shot noise, photoelectron shot noise and camera readout noise. In addition, the image analysis software may add noise if the algorithms are sensitive to changes in the placement of the array in the image. The reproducibility of the data in Figure 7 demonstrated that the measurements are very stable when the detected intensities are high, indicating that variation in illumination intensity integrated over our exposure times, and shot noise from the dark current are negligible. This leaves the photoelectron statistics and camera readout noise, and perhaps software issues, as sources of variation in measurements. All become more important as the amount of collected light for a measurement decreases.

Figure 8 shows the behavior of the data from the same hybridization used in Figure 7 as the exposure times for Cy3 and Cy5 are reduced by a factor of 10 from 20 and

Figure 5. DAPI image of $\sim 30\,000$ element test array. DNA was printed from 864-well microtiter plates (3 mm well spacing) using our custom-built array printer (S. Clark, G. Hamilton, N. Brown, V. Oseroff, R. Nordmeyer, D. Albertson, D. Pinkel, manuscript in preparation). Large numbers of replicate spots were printed for each solution, leading to the stripped appearance which represents differences in the DNA concentrations in the printing solutions. The elements are printed on ~ 95 μm centers. Expanded views of the image from a region at the center and in the lower left corner show the elements are well resolved. The printing pin used at the center of the array produced spots of ~ 60 μm diameter, while that at the lower left made elements with a diameter of ~ 70 μm . Pixel intensities are shown for a vertical line through three spots in the lower left corner for the original image data, and after deconvolution sharpening of the image. The signal level between the elements is due to a combination of camera offset, ~ 220 U, fluorescence from free DAPI in the mounting medium, and slight softness in the image. The softness is seen by the slight elevation of the intensities in the troughs between array elements compared with the intensity in the image outside of the area of the array (pixels 33–39 in this plot). Intensities along diagonal lines connecting the elements fall fully to 'background' levels (data not shown). Deconvolution image sharpening (using a Wiener filter implemented in MATLAB) deepens the troughs to the same level as the region outside the array and improves the resolution of features of spot morphology.

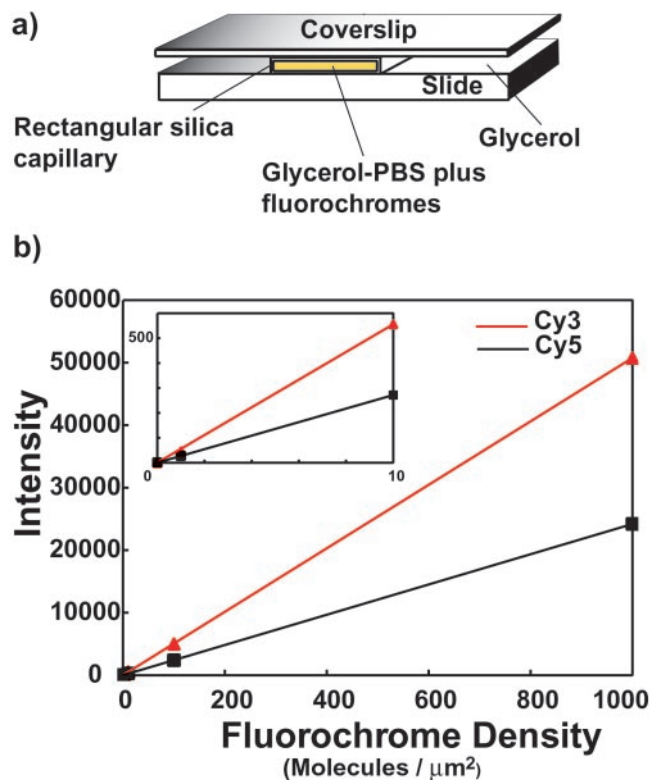


Figure 6. Detection sensitivity. (a) Glycerol-PBS solutions containing known concentrations of Cy3 and Cy5 were loaded into rectangular fused silica capillaries, placed on a chromium-coated microscope slide, surrounded by glycerol and a glass cover slip applied. This mounting closely matched the indices of refraction of capillaries (fused silica ~ 1.459 , glycerol ~ 1.473) so that very little light scatter was generated at the capillary surfaces. Five capillaries were mounted in an image field, each containing a mixture of Cy3 and Cy5 at concentrations of 0, 1, 10, 100 and 1000 molecules/ μm^2 , and Cy3 and Cy5 images acquired. Concentrations of stock solutions were determined using absorbance measurements and known extinction coefficients. (b) Fluorescence intensities Cy3 (red curve) and Cy5 (black curve) increased linearly with fluorochrome density. The inset shows the portion of the curves between 0 and 10 fluorochromes/ μm^2 , indicating the ability to detect concentrations below 1 fluorochrome/ μm^2 .

40 s to 2 and 4 s, respectively, and by a further factor of 10–0.2 and 0.4 s. For the first exposure step there is essentially no change in the data, even in small details. However, increased variation is clearly seen at the lower values of A for the shortest exposure. Plotting these data in genome order, Figure 8b, shows that there is essentially no degradation in the data quality for the first reduction in exposure as compared to Figure 7a, but broadening is clearly visible at the lowest exposure. Eye-ball examination of the overall behavior of Figure 8a indicates that sufficient light is collected so that the imaging system does not contribute significantly to measurement variation if the intensities are $> \sim 2^5 - 2^6 = 32 - 64$. Thus this system can measure ratios with a standard deviation of the Log_2 Ratios < 0.06 over a dynamic range of ~ 1000 . The dynamic range is higher if one relaxes the accuracy standards. Comparison of the measured broadening of the M versus A data in Figure 8 with calculations based on the expected noise in the images due to photoelectron counting statistics and camera readout shows very close agreement, as shown in the inset to Figure 8a and in Figure 9. Details of the calculation of the expected noise

performance of the system are contained in the Supplementary Data. The calculation indicates that camera readout noise is the dominant source of measurement uncertainty in this range of A because the elements on this array are large enough to produce a substantial total number of photoelectrons even when the average intensity of the signal is low. Calculations of noise limits in systems with PMT detectors is more complex because one needs to calibrate the various gain settings in order to relate the signal output of the system to the actual intensity of the detected light. In contrast, with a CCD the signal is related to the amount of collected light by an unchanging constant factor.

DISCUSSION

The imaging system we have described is the third generation in a developmental series (4). We desired to minimize the need to apply computational corrections to the images in order to reduce the risk of introducing systematic errors into the biological results. Thus we chose to image large areas in a single frame with sufficient resolution so that tens of thousands of elements could be distinguished for ‘whole genome’ experiments, and to provide a chromatically stable illumination distribution. Arrays that do not fit into a single image field are analyzed field by field and the data subsequently merged. Composite images of an entire array are produced only for display purposes. While the emphasis here has been on measurements of nucleic acid microarrays, our system has been used also for analysis of proteins (5) and low-resolution imaging of tissue specimens.

The design choices for our system are based on the view that the information from the array is carried in the ratios of the total integrated intensities produced by hybridization to the array elements. Experience has supported this expectation, and we find that many of the array parameters of concern to others, such as uniformity of array element morphology or size, do not substantially affect the results obtained with the arrays that we produce (3,4). Cleanly resolving neighboring array elements and attributing the proper total emission to each is critical, but high-resolution examination of the signal distribution within an array element is not. Several tens of pixels per array element are sufficient to apply general quality control measures to the hybridization, for example the correlation of the different fluorochrome intensities over the element (2). Thus we chose to employ ~ 100 pixels to image an array element and its surrounding background. A high-dynamic range genome-scale measurement involving a tiling path of genomic BAC clones or a complete set of genes requires $\sim 30\text{--}40\ 000$ array elements, would then require an image with $\sim 2\text{K} \times 2\text{K}$ pixels with large electron capacity. We chose a back-thinned CCD in order to obtain the highest possible quantum efficiency. Array printing technology that is based on using standard microtiter plates for holding the printing solutions and on microscope slides as the printing substrate, suggests that a convenient dimension for an array is 18 mm. These criteria require fluorescence detection optics with $\sim 10\ \mu\text{m}$ resolution or better across the entire field. Moreover, we desired to compare more than two nucleic samples simultaneously (6), to use the blue-emitting stain DAPI to identify array elements independently of the hybridization signals, and to simplify

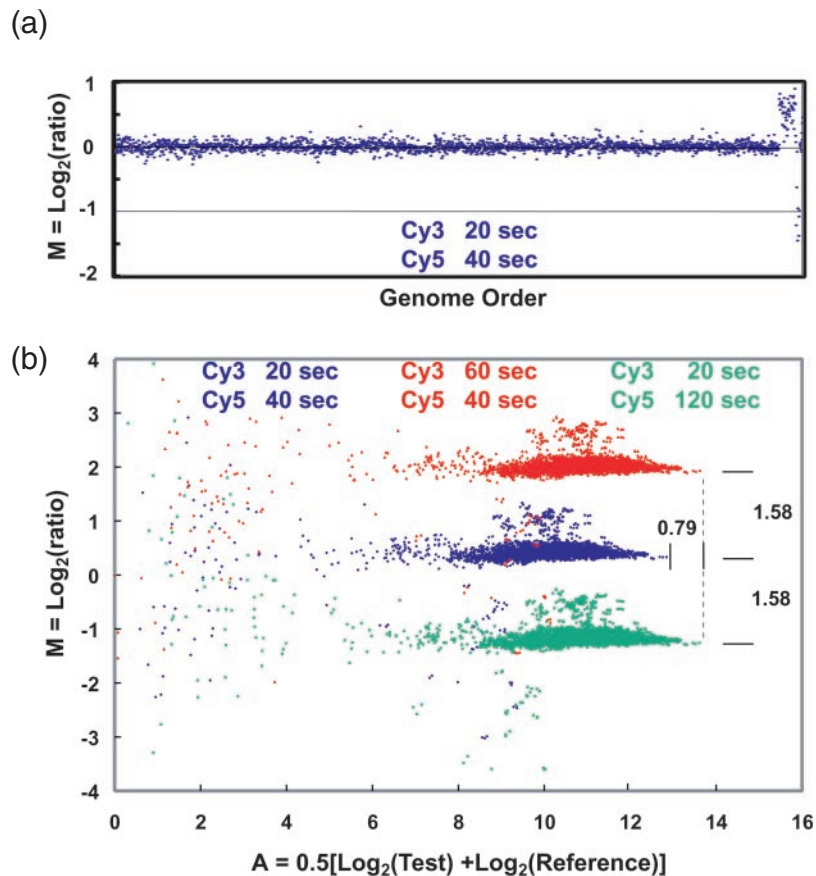


Figure 7. (a) Array CGH comparison of genomic DNA from a normal female to a normal male using a microarray containing BAC clones mapped to ~ 2500 loci distributed across the genome. Each point represents the average value of $M = \text{Log}_2(\text{ratio})$ for the triplicate array elements for each locus, plotted according to its order in the genome. The elevated points to the right are X chromosome loci, and the low points at the very far right are on the Y chromosome. No computational corrections to the images or data, other than an overall normalization so that the median value of $M = 0$, were applied to the images or the data. Exposure times for the Cy3 and Cy5 images are indicated. (b) 'M versus A' plots for all 7500 elements on the array for images acquired with different exposure times. 'A' is a combined measure of the Test and Reference intensities as indicated on the plot. Blue points indicate data from the images used for (a), which were obtained with our 'standard' exposure times. The points above the main band correspond to X chromosome loci, while the few falling below map to loci on the Y. Small clusters of three points can be seen, which are produced by the triplicate elements for each locus. Points in red and green show the results when exposures of the Cy3 or Cy5 have been increased by a factor of 3. Exposure times are shown with a color code to match the data points. The locations of the data points move by exactly the amount expected, $\Delta M = \text{Log}_2(3) = 1.58$, $\Delta A = 0.5\text{Log}_2(3) = 0.79$, as indicated on the plot. Note that the plots for the different exposure times have the same distribution of points to very high accuracy, as can be seen, for example, by the reproducibility of the relative positions of the measurements of loci that fall outside the main cloud. Independent sets of Cy3 and Cy5 images were obtained for each analysis. The data points represent background-corrected intensities obtained directly from the images without computational adjustment or overall normalization.

operations by avoiding refocusing as wavelengths were changed. Our experience with high-quality commercially available photographic (4), television, dissecting microscope lenses and the like in the first generation versions of this imaging system (4) indicated that custom lens designs would be required to meet our performance criteria. Figures 5–8 illustrate the performance of the resulting system, and demonstrate in particular that arrays with many more than 30 000 elements per field can be well imaged.

The maximum number of array elements that can be imaged with this system in its current configuration depends on the desired measurement accuracy. Most array elements in our hybridizations show pixel to pixel intensity correlations of the test and reference signals that are very close to 1.0. This indicates that the ratio on any single pixel within the element would provide a good measurement. The rest are 'redundant', except in so far as one might want to apply quality control criteria. As stated above, the optical resolution of

the current optics keeps essentially all of the light from a sub-resolution point source within a 3×3 block of pixels. The minimum useful spacing between such point sources for a real measurement depends on the intensity variations among the sources, with the most challenging task involving accurate measurement of a dim array element that is next to a bright one. Deconvolution image sharpening, as illustrated in Figure 5, can assist with this task. Given these considerations it seems very likely that high-quality data could be obtained from an array with elements on 50 μm centers, ~ 130 000 elements per image, and perhaps even closer. The measurement precision for such an array can be estimated using the relationship derived in the Supplementary Data and illustrated Figure 9. Assuming an area of 1 pixel for an array element and a typical background level of 200 digital units, the contribution to the standard deviation of the Log_2Ratio from the imaging system should be below 0.1 for signal intensities above ~ 300 . Thus the useful dynamic

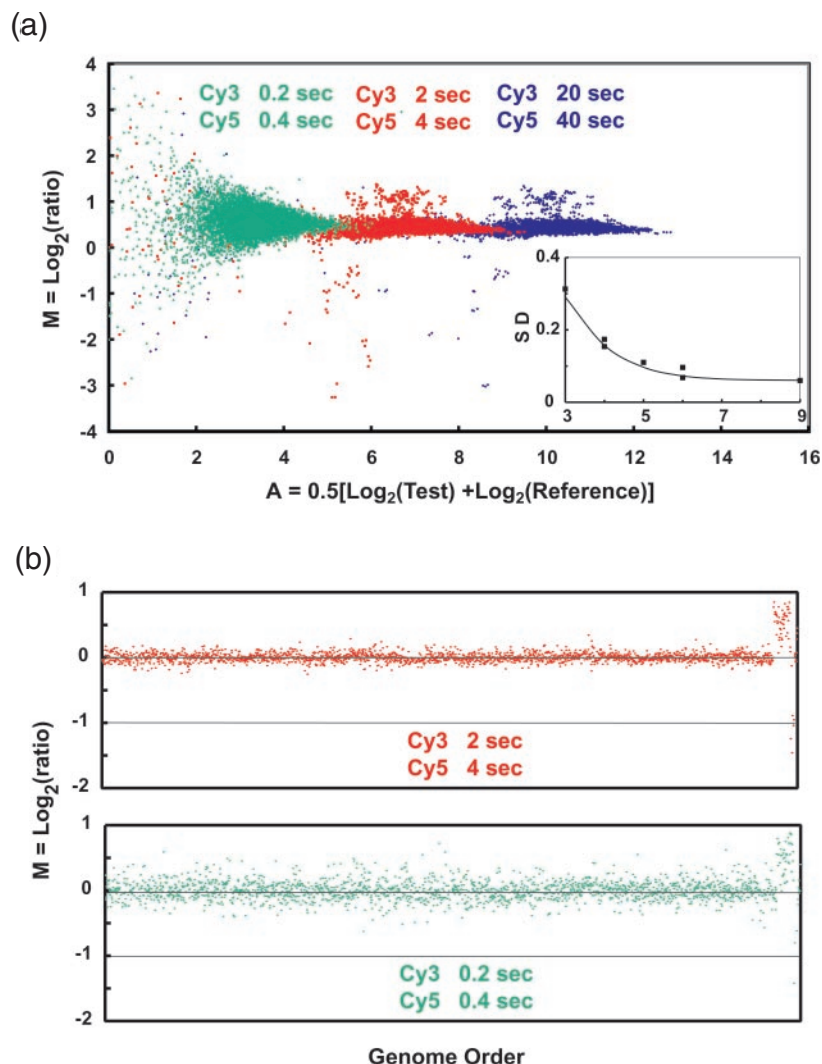


Figure 8. Dependence of measurement precision on signal intensity. (a) M versus A as a function of reduced exposure times. Data from three sets of exposure times, our standard and two steps of 10-fold reduction of both Cy3 and Cy5, are shown for the same array as in Figure 7. Each point represents one element (~ 7500 total) on the array, its color matching the exposure times shown at the top of the figure. Within each exposure the intensities of the elements range over 4 U in A as in Figure 7, and between exposures they decrease by exactly the expected factor of 10. Careful examination of the points that are individually distinguishable in the two highest exposure times show that they have nearly identical relative locations, indicating very low random noise in the entire analytical process. However, broadening in M is clearly seen at the lowest exposure for those elements on the array where the intensity is $< A = 5-6$. No computational adjustments have been made to these data. The inset shows the standard deviation of the $\text{Log}_2(\text{Ratio})$, (standard deviation of M), as a function of A . The points were obtained from an analysis of the data in the main figure, and the line is based on a model that includes photon counting statistics and camera readout noise as the only sources of random variation in the measurement (Supplementary Data). The calculation indicates that camera readout noise makes the dominant contribution to the measurement uncertainty because the array elements are large enough so that their total light emission is sufficient to make photoelectron shot noise less important until even lower intensities. Note that in these measurements the background intensity is effectively zero, since it is reduced proportionally to the signals as the exposure times are reduced. Thus they do not accurately simulate an actual measurement situation. An enlarged view of this inset, including additional curves modeling the effects of constant background levels as well as very small array elements, is shown in Figure 9. (b) Copy number profiles for the data from the two lowest exposures. The profile (red points) is very similar to that of Figure 7a, which was obtained with a 10-fold higher exposure time. The profile for the lowest exposure clearly shows broadening, and many points have been removed by quality control filtering. Even so, the basic copy number features are clearly present with exposures that are 100-fold lower than 'standard'.

range of the system, assuming this accuracy criterion, would be ~ 200 , and could be extended substantially by summing multiple images.

The imaging system contributes two sources of 'background' that must be removed during analysis in order to obtain the most accurate results—the inherent offset of the camera output, and light originating from the array substrate and the coverslip. Figure 2 illustrates typical magnitudes of the

offset and background in our system for standard measurement configurations. Our image analysis employs the common technique of subtracting the local background from the intensity of an array element prior to calculating fluorescence ratios. The appropriateness of local background subtraction for these images is evident in Figures 7 and 8, where the ' M versus A ' plots remain straight and essentially identical for a wide range of exposure times without employing computational

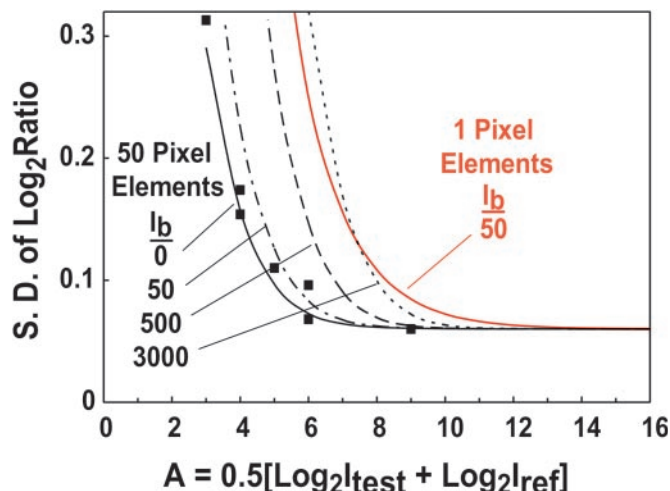


Figure 9. Estimation of ratio measurement precision for different conditions. The closed square boxes indicate measured values of the standard deviation of the $\text{Log}_2(\text{ratio})$ as a function of $\text{Log}_2(\text{intensity})$, A , from the data in Figure 8a. The 'intrinsic' variation in this array, as determined by the standard deviation measured at high intensity, is 0.06. The solid black line shows the behavior of the model calculation using the camera and array parameters appropriate for these measurements. The data points and predicted behavior are also shown in the inset of Figure 8a. In these measurements the background intensity is effectively 0, since it is reduced proportionally to the signals as the exposure times are reduced to get the low intensity signals. This is not an accurate simulation of a true measurement because detection of truly weak signals requires longer exposures and their concomitant higher backgrounds. The black dotted lines indicate the expected measurement precision for background light levels of 50, 500 and 3000 digital units. For typical exposures one expects minimum backgrounds of ~ 50 – 100 based on the data in Figure 2. Thus when the signal intensities are ~ 62 digital units ($A = 6$) above the background, the measurements approach 0.06, the 'intrinsic' variation in the array in this simulation. The solid red line simulates the expected measurement resolution for an array in which all of the light from an array element is collected in one pixel, background is determined from 15 nearby pixels, and the background level is 50 digital units. The standard deviation of the Log_2 ratios is predicted to be <0.1 for intensities $>>300$ digital units above background.

corrections that are frequently instituted in array analysis (8). The uniform backgrounds produced by some array substrates and coverslips, while esthetically displeasing, have limited impact on data quality. The contribution of a background to the measurement noise level arises through the uncertainty in establishing the level to subtract, which is fundamentally determined by photoelectron shot noise from the background. The predicted effect of a wide range of background levels is illustrated in Figure 9.

Subtraction of local background has a problematic aspect since it also subtracts background due to non-specific binding of the labeled nucleic acids to the array substrate. This correction may not be accurate because the non-specific affinities of the substrate and the array elements are likely to be different, as evidenced the occurrence of hybridizations in which the substrate affinity is so high that it is brighter than the array elements. The amount of this background signal can be estimated using the data in Figure 2 to determine the contribution from the camera offset and bare substrates, and subtracting that from the measured background levels. If the signal from the non-specific binding to the substrate is a substantial fraction of the apparent signal on the array elements, data quality may be compromised.

The maximum useful sensitivity of an array-imaging instrument is determined by the distribution of fluorescent contaminants in the measurement environment, including autofluorescence from the array elements and the like. Once these can be detected, increases in system sensitivity will not result in improved data since the measurement problem is not signal detection, but distinguishing the portion of the signal that represents the desired hybridization from the rest of the emission sources. Better data require improved experimental technique related to array production and hybridization, not increased instrument sensitivity. Figure 6 demonstrated that our instrument maintains a linear response down to fluorochrome densities well below $1 \text{ molecule}/\mu\text{m}^2$, corresponding to tens of molecules per pixel. This limit was set by difficulty in producing a cleaner measurement environment. Extended integration times would allow us in principle to detect single fluorochromes, but the large pixel size results in a substantial number of other weakly emitting molecules in the pixel that overwhelm the desired signal.

The performance of the imaging system described here can serve to estimate what could be achieved with different designs that meet different optimization criteria. Alternative choices for excitation source and design of the excitation optics could improve performance and operational convenience, and potentially reduce cost. With the current system, adding anti-reflection coatings on the surfaces of the four elements of Lens 1 and on Lens 2, increasing the proportion of the excitation beam used for illumination by reducing the focal length of Lens 3, and using the reflector system to return excitation light to the array for a second pass, could increase the effective excitation intensity by more than a factor of 5, but at the potential cost of needing to institute computational corrections for chromatic variation in the illumination pattern. These changes would reduce the routine exposure times sufficiently so that the camera readout time, currently 4 s, would be a significant factor in determining the data acquisition rate. Given these simple changes, it should be possible to acquire DAPI, Cy3 and Cy5 images at >3 fields per minute. Alternative excitation designs using non-imaging optics, and potentially light emitting diode sources, might provide even higher useful illumination levels and/or operational simplicity compared to the arc lamp and imaging optics of the current excitation system.

The current detection optics are capable of collecting more than enough light to reach the practical sensitivity limits of arrays we are now using. These lenses were designed in two phases, with the more recently designed 105 mm focal length lens having reduced chromatic aberrations compared with the other two. Updating the design of the other lenses would slightly increase the performance of the current system, most notably by extending the useful wavelength range. Changing the optical design to increase the aperture would potentially allow compensating reductions in performance of other components of the system by collecting more light, but keeping the lens aberrations to acceptable levels would be difficult and expensive. Alternatively, reducing the aperture somewhat would reduce the lens costs and not compromise resolution since the current resolution is set by aberrations and not diffraction.

The camera used in this system provides quantum efficiencies $>90\%$ across the useful spectral region, has a large

electron capacity for high dynamic range imaging, and is cooled to allow long integration times. We chose this camera so that we could obtain measurement accuracy of a few percent over a dynamic range of >1000 in signal intensity. The dynamic range can be extended if necessary by reducing the readout noise by slowing the readout time or using electron multiplying readout methods (Andor Technology EMCCD cameras), and/or summing multiple images. However, many applications have sufficiently intense signals and dynamic ranges limited to ~ 2 orders of magnitude, so that a lower performance, less expensive, camera would be adequate. If the excitation intensity, camera readout rate, and the speed of the stage and filter wheels were increased, and microarrays with element densities that exploited the full-resolution capability of the optics were employed, highly quantitative multi-fluorochrome data could be obtained from tens of thousands of array elements per second with a CCD array imaging system.

SUPPLEMENTARY DATA

Supplementary Data are available at NAR Online.

ACKNOWLEDGEMENTS

We thank Jay Reichman, Wim Auer and Paul Millman of Chroma Technology for custom filter design; Colin Coates of Andor Technology for advice on CCD cameras; and Michel Nederlof of Media Cybernetics for system integration. This work was supported by grants R01 CA83040 and U01 CA84118, and by Abbott Molecular Diagnostics. Funding to

pay the Open Access publication charges for this article was provided by research support from Abbott Molecular Diagnostics.

Conflict of interest statement. None declared.

REFERENCES

1. Che,D., Bao,Y. and Muller,U.R. (2001) Novel surface and multicolor charge coupled device-based fluorescent imaging system for DNA microarrays. *J. Biomed. Opt.*, **6**, 450–456.
2. Jain,A.N., Tokuyasu,T.A., Snijders,A.M., Segraves,R., Albertson,D.G. and Pinkel,D. (2002) Fully automatic quantification of microarray image data. *Genome Res.*, **12**, 325–332.
3. Snijders,A.M., Nowak,N., Segraves,R., Blackwood,S., Brown,N., Conroy,J., Hamilton,G., Hindle,A.K., Huey,B., Kimura,K. *et al.* (2001) Assembly of microarrays for genome-wide measurement of DNA copy number. *Nature Genet.*, **29**, 263–264.
4. Pinkel,D., Segraves,R., Sudar,D., Clark,S., Poole,I., Kowbel,D., Collins,C., Kuo,W.L., Chen,C., Zhai,Y. *et al.* (1998) High resolution analysis of DNA copy number variation using comparative genomic hybridization to microarrays. *Nature Genet.*, **20**, 207–211.
5. Shingyoji,M., Gerion,D., Pinkel,D., Gray,J.W. and Chen,F. (2005) Quantum dots-based reverse phase protein microarray. *Talanta*, **67**, 472–478.
6. Pinkel,D. and Albertson,D.G. (2005) Array comparative genomic hybridization and its applications in cancer. *Nature Genet.*, **37**, S11–17.
7. Wittrup,K.D., Westerman,R.J. and Desai,R. (1994) Fluorescence array detector for large-field quantitative fluorescence cytometry. *Cytometry*, **16**, 206–213.
8. Yang,Y.H., Dudoit,S., Luu,P., Lin,D.M., Peng,V., Ngai,J. and Speed,T.P. (2002) Normalization for cDNA microarray data: a robust composite method addressing single and multiple slide systematic variation. *Nucleic Acids Res.*, **30**, e15.